ACS Sustainable Chemistry & Engineering

pubs.acs.org/journal/ascecg



Research Article

# Combining High-Throughput Experiments and Active Learning to Characterize Deep Eutectic Solvents

Dinis O. Abranches, William Dean, Miguel Muñoz, Wei Wang, Yangang Liang, Burcu Gurkan, Edward J. Maginn, and Yamil J. Colón*

Cite This: *ACS Sustainable Chem. Eng.* 2024, 12, 14218−14229

Read Online

ACCESS | Metrics & More | Article Recommendations | Supporting Information

**ABSTRACT:** The high tunability of deep eutectic solvents (DESs) stems from the ease of changing their precursors and relative compositions. However, measuring the physicochemical properties across large composition and temperature ranges, necessary to properly design target-specific DESs, is tedious and error-prone and represents a bottleneck in the advancement and scalability of DES-based applications. As such, active learning (AL) methodologies based on Gaussian processes (GPs) were developed in this work to minimize the experimental effort necessary to characterize DESs. Owing to its importance for large-scale applications, the reduction of DES viscosity through the addition of a low-molecular-weight solvent was explored as a case study. A high-throughput experimental screening was initially performed on nine different ternary DESs. Then, GPs were successfully trained to predict DES viscosity from its composition and temperature, showcasing the ability of these stochastic, nonparametric models to accurately describe the physicochemical properties of complex mixtures. Finally, the ability of GPs to provide estimates of their own uncertainty was leveraged through an AL framework to minimize the number of data points necessary to obtain accurate viscosity modes. This led to a significant reduction in data requirements, with many systems requiring only five independent viscosity data points to be properly described.

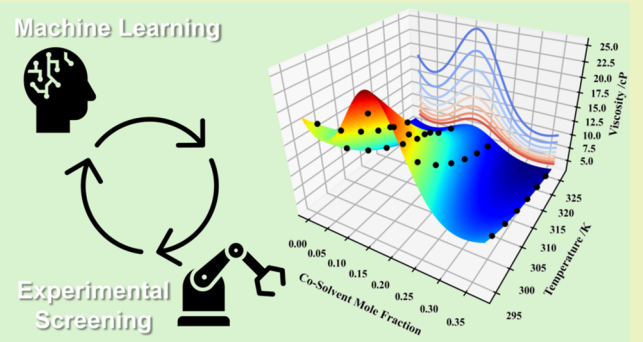


**KEYWORDS:** *machine learning, Gaussian processes, viscosity, choline chloride, ethaline*

## INTRODUCTION

Deep eutectic solvents (DESs) are a novel class of sustainable solvents.[1,2] They are eutectic-type liquid mixtures prepared by physically mixing solid precursors, usually a hydrogen bond donor (HBD) and a hydrogen bond acceptor (HBA), without the need for any chemical reaction or synthesis steps. The liquid phase of a DES arises due to the establishment of a solid−liquid equilibrium where its components are strongly interacting, usually through the formation of extensive hydrogen-bonding networks.[1,2] Thus, the notion of DESs greatly expands the amount and type of compounds available as liquid solvents by allowing solid precursors, otherwise unfit for solvation processes, to form liquid phases at a given desired temperature (typically room temperature).

Because DESs are mixtures, their properties, which are directly connected to those of their precursors, can be easily tuned by simply changing the relative composition of each component. This high degree of tunability, combined with desirable sustainability metrics,[3] has led to the successful application of DESs in a variety of chemistry-related areas, such as carbon dioxide capture,[4,5] extraction of bioactive and value-added compounds,[6−9] metal oxide dissolution and processing,[10,11] and drug formulation and delivery.[12,13] DESs also find applications as solvents for electrochemical processes and energy storage,[14,15] particularly under the umbrella of concentrated hydrogen-bonded electrolytes (CoHBEs) in redox flow batteries.[16,17]

Despite their usefulness and overall green character, DESs typically display high viscosities, stemming from both the usage of solid precursors in their preparation and the formation of extensive hydrogen-bonding networks.[18,19] For example, commonly studied DESs such as the 1:2 molar ratio mixtures of choline chloride and urea or ethylene glycol exhibit viscosities that are 2−3 orders of magnitude higher than those of typical solvents (e.g., water or ethanol).[20,21] This major drawback, which hampers the deployment of DESs in industrial applications, is commonly mitigated by modulating DES viscosity through the addition of a low-molecular-weight cosolvent as a third component (e.g., water).[18,21,22] A great

Received: June 1, 2024
Revised: August 26, 2024
Accepted: August 27, 2024
Published: September 10, 2024

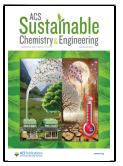

deal of research has been done focusing on the impact of this cosolvent in the structure and intermolecular interactions of DESs.[23]

While tunability is a key advantage of DESs, the necessity of using cosolvents to adjust their properties, particularly viscosity, adds an extra dimension to an already vast design space that encompasses operational conditions (e.g., temperature) and the chemical natures and relative compositions of HBD and HBA precursors. Furthermore, anticipating the behavior of DESs upon cosolvent addition is not a trivial task, which is exacerbated by a lack of available theoretical or even empirical models that can describe DES properties beyond simple temperature dependencies. The literature reflects this, with most DES-targeted viscosity models proposed to date attempting to describe only simple temperature dependencies.[24,25] As such, the current design framework of novel DESs is limited by tedious experimental viscosity measurement campaigns on ternary systems across large composition and temperature ranges.[18]

Gaussian processes (GPs) are machine learning (ML) models that excel as interpolators of data and are quickly becoming decisive tools in several chemistry-related fields.[26,27] They are versatile, nonparametric models that are easy to use and implement and do not assume any underlying functional form between dependent and independent variables. We have recently shown the feasibility of using GPs to accurately describe the activity coefficients of organic mixtures, including DESs, which, in turn, allows for the prediction of a plethora of phase equilibrium phenomena.[28] Another advantage of GPs is their stochastic nature, through which they can provide blind uncertainty estimates for their own predictions. This allows the use of active learning (AL) algorithms to iteratively build GP models for a given application. That is, AL can guide the design of experiments and acquisition of data in an efficient manner, greatly reducing the number of experimental measurements necessary to construct accurate models.[28,29]

To fast-track the design and development of low-viscosity DESs, this work illustrates how high-throughput experimentation and AL can be combined to comb through a variety of DES precursors, cosolvents, and operational conditions quickly and efficiently. To do so, a high-throughput experimental screening was initially performed on nine different ternary DESs, composed of choline chloride (ChCl) as the HBA, ethylene glycol (EG) or aniline (AN) as the HBDs, and water ($H_2O$), acetonitrile (ACN), or dimethyl sulfoxide (DMSO) as the cosolvents. These DES components were chosen based on their previous study and usage for energy storage applications,[30] as well as their different and complex viscosity trends. Then, with the aim of obtaining a general framework to accurately model the viscosity of ternary DESs, GP models were developed to describe the viscosity of the studied DESs as a function of their composition and temperature. Finally, the ability of GPs to provide estimates of their own uncertainty was leveraged as part of AL algorithms to greatly minimize the amount of experimental high-throughput data points necessary to obtain accurate viscosity models.

## METHODS

This section describes the experimental and computational methods employed in this work. All Python codes developed and deployed are available, free of charge, in the following GitHub repository: https://github.com/MaginnGroup/ViscAL.

**Materials.** Unless otherwise specified, all solvents were used without further purification. The hydrogen bond acceptor—choline chloride (99% purity)—and the hydrogen bond donors—anhydrous ethylene glycol (99.8% purity) and aniline (99.5% purity)—were purchased from Sigma-Aldrich. Anhydrous solvents—acetonitrile (99.8% purity) and dimethyl sulfoxide (99.8% purity)—were also from Sigma-Aldrich. Deionized water was obtained with a Milli-Q apparatus (water resistivity of 18.2 MΩ·cm at 298 K and total organic carbon < 5 ppb).

**Mixture Preparation.** DESs were prepared by mixing the HBA (choline chloride) and the desired HBD in either a 1:4 or a 1:6 molar ratio (ChCl:HBD) while stirring at 80 °C for 1 h using a modular robotic platform (Big Kahuna, Unchained Laboratories) inside an argon-filled glovebox.[30−32] Samples were then cooled to room temperature and mixed with a cosolvent (water, acetonitrile, or dimethyl sulfoxide) using a vortexer. The final molar ratios of the ternary ChCl:HBD:cosolvent mixtures were 1:4:0.5, 1:4:1, 1:4:2, or 1:4:4. Mixtures of ChCl:AN:cosolvent in molar ratios of 1:6:0.5, 1:6:1, 1:6:2, and 1:6:4 were also prepared. These compositions follow those already extensively studied for energy storage applications.[30]

**Viscosity Measurements and Modeling.** All viscosity measurements were performed using a VROC initium one plus high-throughput viscometer (RheoSense), with temperatures ranging from 298 to 323 K (±0.1 K) in 5 K increments.[30] All measurements were repeated at least 3 times, with means and standard deviations reported in Tables S1−S4. The Vogel−Fulcher−Tammann (VFT) equation was used to model the data collected in this work[33]

$$\eta = \eta_o \exp\left(\frac{B}{T - T_o}\right) \tag{1}$$

where $\eta$ is the observed viscosity at temperature $T$, and $B$, $\eta_o$, and $T_o$ are the empirical fitting parameters. Equation 1 was fitted to all data sets using a nonlinear least-squares approach.

**Gaussian Processes.** In this work, GPs were used to describe viscosity ($\eta$) as a function of composition (mole fractions, $x_i$) and temperature ($T$). Thus, for each case, a surrogate function $\eta'(\boldsymbol{X})$ was constructed and distributed as a GP with the mean function $m(\boldsymbol{X})$ and covariance function $k(\boldsymbol{X})$[26,34]

$$\eta'(\boldsymbol{X}) \sim \mathcal{GP}[m(\boldsymbol{X}), k(\boldsymbol{X})] \tag{2}$$

where $\boldsymbol{X}$ is the feature vector containing the input variables ($\boldsymbol{X} = [x_1, x_2, x_3, T]$). The mean and covariance functions encode information about the relationship between viscosity and composition/temperature. Following previous results obtained for other physicochemical properties of DESs,[28] and to simplify the training and usage of the GPs studied in this work, the mean function was taken to be zero, i.e., $m(\boldsymbol{X}) = 0$.

Two popular covariance functions (also known as kernels)—the radial basis function (RBF) kernel and the rational quadratic (RQ) kernel—were tested in this work.[35] These are defined as[36]

$$\mathrm{RBF}(\boldsymbol{X}_i, \boldsymbol{X}_i) = \sigma^2 \exp\left(-\frac{\|\boldsymbol{X}_i - \boldsymbol{X}_j\|^2}{2l^2}\right) \tag{3}$$

$$\mathrm{RQ}(\boldsymbol{X}_i, \boldsymbol{X}_j) = \sigma^2\left(1 + \frac{\|\boldsymbol{X}_i - \boldsymbol{X}_j\|^2}{2\alpha l^2}\right)^{-\alpha} \tag{4}$$

where $\sigma$ and $l$ are the variance and length-scale parameters of the kernel, respectively, $\mathrm{a}\|\boldsymbol{X}_i - \boldsymbol{X}_j\mathrm{a}\|$ represents the Euclidian distance between $\boldsymbol{X}_i$ and $\boldsymbol{X}_j$, and $\alpha$ is an RQ-specific hyperparameter. Regardless of the main kernel chosen eqs 3 or 4, a white noise kernel ($W$) was also used to account for experimental uncertainty[35,36]

$$W = k(\boldsymbol{X}_i, \boldsymbol{X}_j) = \delta(i, j)\sigma^2 \tag{5}$$

where $\delta(i,j)$ is one when $I = j$ and zero otherwise.

Given $N$ training data points, the GP represented by eq 2 can be fitted, and a new viscosity data point predicted through



https://doi.org/10.1021/acssuschemeng.4c04507
ACS Sustainable Chem. Eng. 2024, 12, 14218−14229

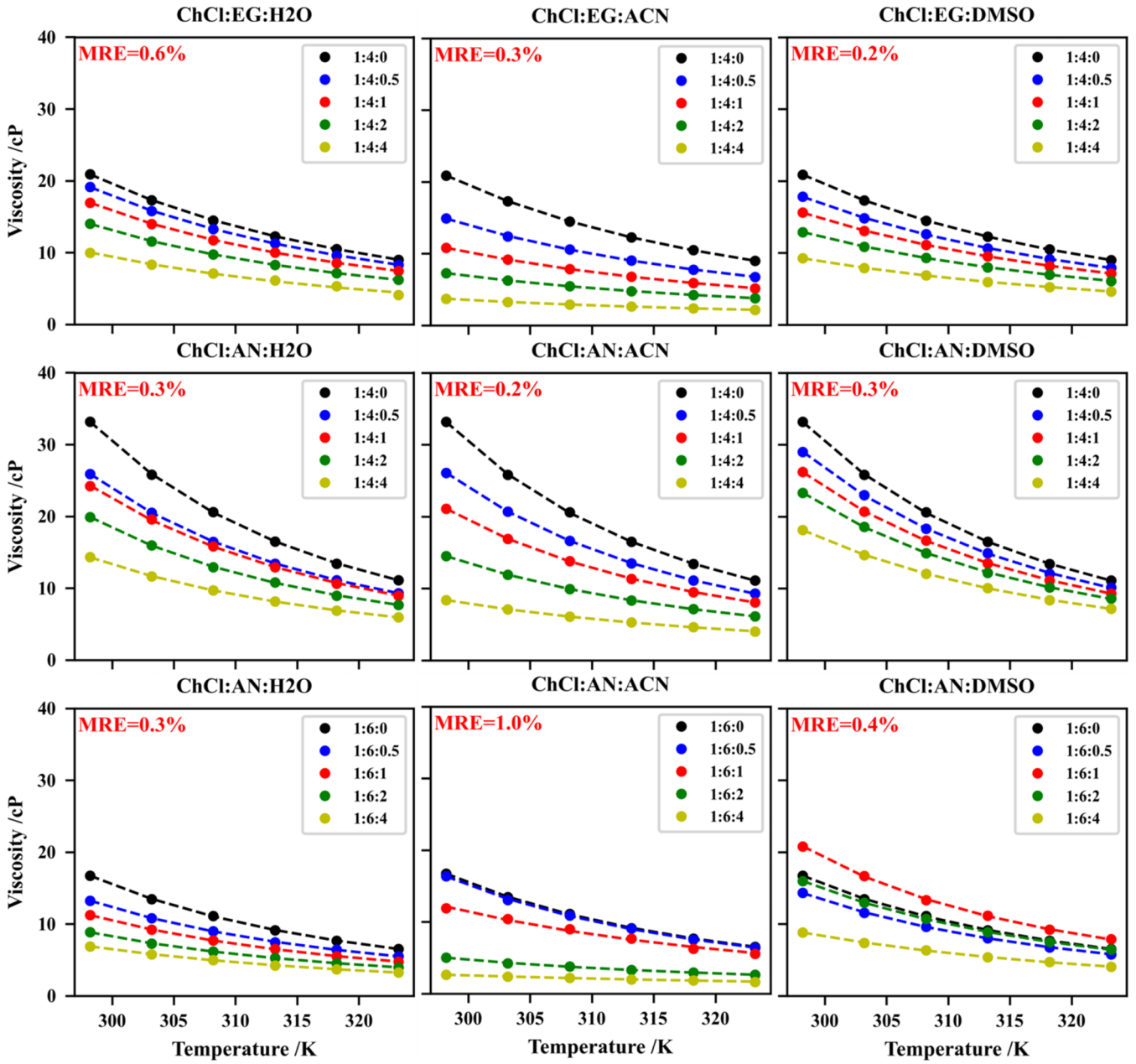


**Figure 1.** Experimental high-throughput viscosity data measured in this work (circles) for ternary deep eutectic solvents, namely, those based on ChCl:EG (1:4) (top row), ChCl:AN (1:4) (middle row), and ChCl:AN (1:6) (bottom row), with added water (left column), acetonitrile (middle column), and dimethyl sulfoxide (right column). Colors indicate different cosolvent mole ratios, and dashed lines represent VFT fits, with their mean relative errors (MREs) being provided as the inset.

$$\begin{bmatrix} \eta_1 \\ \vdots \\ \eta_N \\ \eta_i' \end{bmatrix} \sim \mathcal{N}(0, \boldsymbol{\Sigma}) = \mathcal{N}\left( \begin{bmatrix} 0 \\ \vdots \\ 0 \\ 0 \end{bmatrix}, \begin{bmatrix} \boldsymbol{\Sigma}_{\eta,\eta} = \begin{bmatrix} k(\boldsymbol{X_1}, \boldsymbol{X_1}) & \cdots & k(\boldsymbol{X_N}, \boldsymbol{X_1}) \\ \vdots & \ddots & \vdots \\ k(\boldsymbol{X_1}, \boldsymbol{X_N}) & \cdots & k(\boldsymbol{X_N}, \boldsymbol{X_N}) \end{bmatrix} & \boldsymbol{\Sigma}_{\eta,\eta_i'} = \begin{bmatrix} k(\boldsymbol{x_i}', \boldsymbol{X_1}) \\ \vdots \\ k(\boldsymbol{x_i}', \boldsymbol{X_N}) \end{bmatrix} \\ \boldsymbol{\Sigma}^{\boldsymbol{T}}_{\eta,\eta_i'} = [k(\boldsymbol{X_N}, \boldsymbol{X'}_{\boldsymbol{i}}) \quad \cdots \quad k(\boldsymbol{X_N}, \boldsymbol{X'}_{\boldsymbol{i}})] & \boldsymbol{\Sigma}_{\eta_i',\eta_i'} = k(\boldsymbol{X'}_{\boldsymbol{i}}, \boldsymbol{X'}_{\boldsymbol{i}}) \end{bmatrix} \right) \tag{6}$$

where $\mathcal{N}(0, \boldsymbol{\Sigma})$ represents a multivariate Gaussian distribution with mean zero and covariance $\sum$, which is subdivided into the covariances between known training data points ($\sum_{\eta,\eta}$), unknown testing data points ($\sum_{\eta_i',\eta_i'}$), and cross-covariances ($\sum_{\eta,\eta_i'}$ and $\sum^{T}_{\eta,\eta_i'}$). Within the framework of GPs, the unknown variable $\eta_i'$ is treated as a random variable jointly distributed with the training data, such that

$$\eta_i' | \boldsymbol{\eta} \sim \mathcal{N}(\mu', \Sigma') \tag{7}$$

with $\mu'$ and $\sum'$ being

$$\mu' = \boldsymbol{\Sigma}^{\boldsymbol{T}}_{\eta,\eta_i'} \boldsymbol{\Sigma}^{-1}_{\eta,\eta} \boldsymbol{\eta} \tag{8}$$



https://doi.org/10.1021/acssuschemeng.4c04507
ACS Sustainable Chem. Eng. 2024, 12, 14218−14229

$$\Sigma' = \Sigma_{\eta_i',\eta_i'} - \mathbf{\Sigma}^{T}_{\eta,\eta_i'}\mathbf{\Sigma}^{-1}_{\eta,\eta}\mathbf{\Sigma}_{\eta,\eta_i'} \quad (9)$$

Thus, $\mu'$ eq 8 represents the GP-predicted viscosity ($\eta_i'$) at the testing point $\boldsymbol{X}'_i$ (which contains the desired testing compositions and temperature) and $\sum'$ eq 9 represents the GP-predicted uncertainty (variance) of its own viscosity estimate.

In this work, all GP-related calculations were performed using the Python packages GPFlow (V. 2.5.2)[36] and TensorFlow (V. 2.10.0).[37,38] A Gaussian likelihood hyperparameter alongside the white noise kernel eq 5 was used to account for experimental uncertainty. This assumes that the training data have some associated uncertainty ($\varepsilon$) that follows a Gaussian distribution, $\varepsilon N(0,\sigma^2)$, with $\sigma^2$ being a tunable hyperparameter. Note that this parameter ($\sigma^2$) is known as the Gaussian likelihood of the model and its value is added to the diagonal of $\sum_{y,y}$. Thus, each GP model trained in this work possesses between four and five hyperparameters (2 or 3 from the main kernel, the variance of the white noise kernel, and the Gaussian likelihood variance). These were optimized by maximizing the log marginal likelihood of each GP using the L-BFGS-B algorithm.[39]

Finally, features and labels were normalized in this work following usual procedures in the ML literature, which have been shown to be relevant for GP-related DES applications.[28] Different normalization schemes were tested, namely, min−max scaling eq 10, standardization eq 11, and log-standardization eq 12

$$y' = \frac{y - y_{\min}}{y_{\max} - y_{\min}} \quad (10)$$

$$y' = \frac{y - \langle y \rangle}{s_y} \quad (11)$$

$$y' = \frac{\ln(y) - \langle \ln(y) \rangle}{s_{\ln(y)}} \quad (12)$$

where $y'$ is the normalized version of $y$, $y_{\min}$ and $y_{\max}$ are the minimum and maximum values of $y$, $\langle y \rangle$ and $s_y$ represent the mean and standard deviation of $y$, respectively, and $\langle \ln(y) \rangle$ and $s_{\ln(y)}$ represent the mean and standard deviation of the transformed variable $\ln(y)$, respectively. Note that among other benefits, normalization rescales the viscosity data, mitigating the consequences of choosing a GP mean function of zero eq 2, which infers that the expected average DES viscosity value is zero.

## RESULTS AND DISCUSSION

**Viscosity Data.** The viscosity data measured in this work are reported in the Supporting Information (SI) for the binary DESs studied (Table S1), EG-based ternary systems (Table S2), and AN-based ternary systems (Tables S3 and S4). These data are depicted in Figure 1 along with the VFT eq 1 fits obtained.

The viscosity value of neat ChCl:EG (1:4) measured here at 298.15 K, $\eta$ = 20.89 cP, aligns closely with previous reports within the uncertainty associated with the residual water uptake from air during measurements: $\eta$ = 20.84 cP,[40] 24.7 cP (0.05 wt % $H_2O$),[41] and 26.21 cP.[19] The discrepancy in viscosity values can also be attributed to the purity differences in parent compounds. The observed decrease in viscosity with increasing cosolvent addition for ChCl:EG (1:4) also aligns with findings from previous studies on combinations of DESs with $H_2O$,[42−44] ACN,[45] or DMSO.[46] This validates the effectiveness of the high-throughput methodology employed in this work to efficiently measure the viscosity of the studied DESs.

The low intrinsic viscosity of the cosolvents ($\eta_{ACN}$ = 0.34 cP, $\eta_{H_2O}$ = 0.89 cP, and $\eta_{DMSO}$ = 1.99 cP at 298 K),[43,47,48] along with their capability to disrupt or weaken the hydrogen-bonding network among the HBA and HBD components, assists in lowering the overall viscosity of the studied DESs.[30] For instance, Alfurayj et al.[42] demonstrated that the addition of water to ChCl:EG (1:2) in the 1−28.5 wt % range resulted in the solvation of chloride by water, thus disrupting the strong hydrogen-bonding network between this anion and EG. This disruption frees the faster solvent component, EG, thus enhancing solvation dynamics and increasing the overall polarity of the system. A similar behavior has been described when DMSO is employed as a cosolvent in ChCl:EG mixtures.[46,49]

Finally, the results reported in Figure 1 reveal a significant decrease in viscosity with increasing temperature for all systems studied, which is most significant in the ternary mixtures based on ChCl/AN (1:4). Interestingly, temperature has a lower impact on the viscosity of acetonitrile-based systems with cosolvent mole ratios of 3 or 4. The data fit well to the VFT equation, with the largest mean relative errors (MREs) being observed for ChCl:AN:ACN (1.0%), followed by ChCl:EG:$H_2O$ (0.6%) and ChCl:AN:DMSO (0.4%).

**GP Regression.** While the VFT model accurately fits the temperature dependence of viscosity, the lack of models that can capture the composition dependency of viscosity in DESs hampers a thorough analysis of the experimental data collected so far, particularly from the perspective of cosolvent efficiency in decreasing DES viscosities. In this section, we describe how GP regression was performed, aiming at obtaining accurate relationships between DES viscosities and their compositions and temperatures, with all models explored being of the form

$$\eta = \mathrm{GP}(x_1, x_2, x_3, T) \quad (13)$$

where $x_1$, $x_2$, and $x_3$ are the HBA, HBD, and cosolvent mole fractions, respectively. Note that for ternary systems, only two of the three composition parameters ($x_1$, $x_2$, and $x_3$) are independent. When the HBD/HBA ratio of the DES is kept constant, the number of independent composition values decreases to one. Thus, the number of GP input variables in this work could be reduced to just two (e.g., $x_3$ and $T$). However, we chose to use eq 13 with explicit composition variables due to its generality, allowing all methods developed here to be readily deployed to any other systems of interest without modifications, including systems beyond ternary. Moreover, unlike parametric models (such as the VFT equation), increasing the number (i.e., dimensionality) of input variables does not increase the number of GP hyperparameters, which is solely determined by the choice of kernel.

While GPs are nonparametric models, the choice of kernel eqs 3 or 4 and normalization procedures eqs 10−12 can affect their performance.[28] As such, a small benchmark was conducted to probe the best combination of kernels and normalization schemes. To do so, all possible combinations of kernels and normalization procedures were tested on the nine DES ternary systems described in the previous section, with the mean relative errors obtained for each case being reported in Table S5. Note that MREs were calculated by considering all training data, akin to those reported in the previous section for the VFT fits. As Table S5 indicates, MREs are usually higher for GPs with the RQ kernel, with the average MRE of RBF-based GPs being 1.25%, while that of RQ-based GPs being 4.21%. With regard to feature normalization, min−max provides the lowest average MRE (2.38%), followed by standardization (2.60%) and no feature normalization



https://doi.org/10.1021/acssuschemeng.4c04507
ACS Sustainable Chem. Eng. 2024, 12, 14218−14229

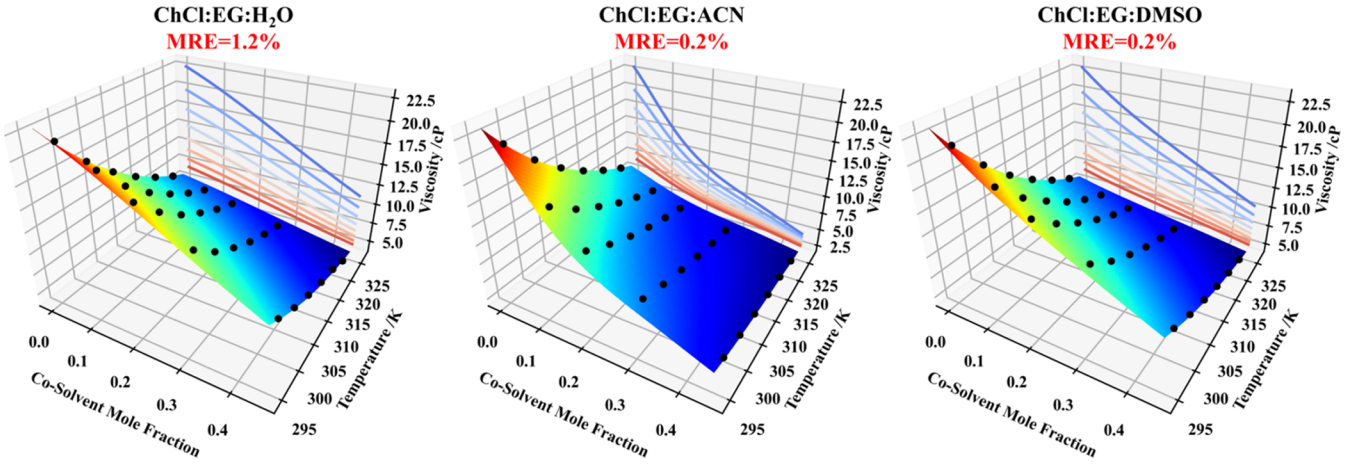


**Figure 2.** Three-dimensional surface plots of the GP-predicted viscosity of ChCl:EG:$H_2O$ (left panel), ChCl:EG:ACN (middle panel), and ChCl:EG:DMSO (right panel) as a function of cosolvent composition and temperature. Color warmth on the surface corresponds to increasing viscosity. Projections of the surface on the composition/viscosity plane are also included, with color warmth corresponding to an increasing temperature. GPs were trained using an RBF kernel (with a white noise kernel and a trainable Gaussian likelihood) against min−max-scaled features and log-standardized labels, with MREs being provided for each case. Black circles indicate experimental GP training data.

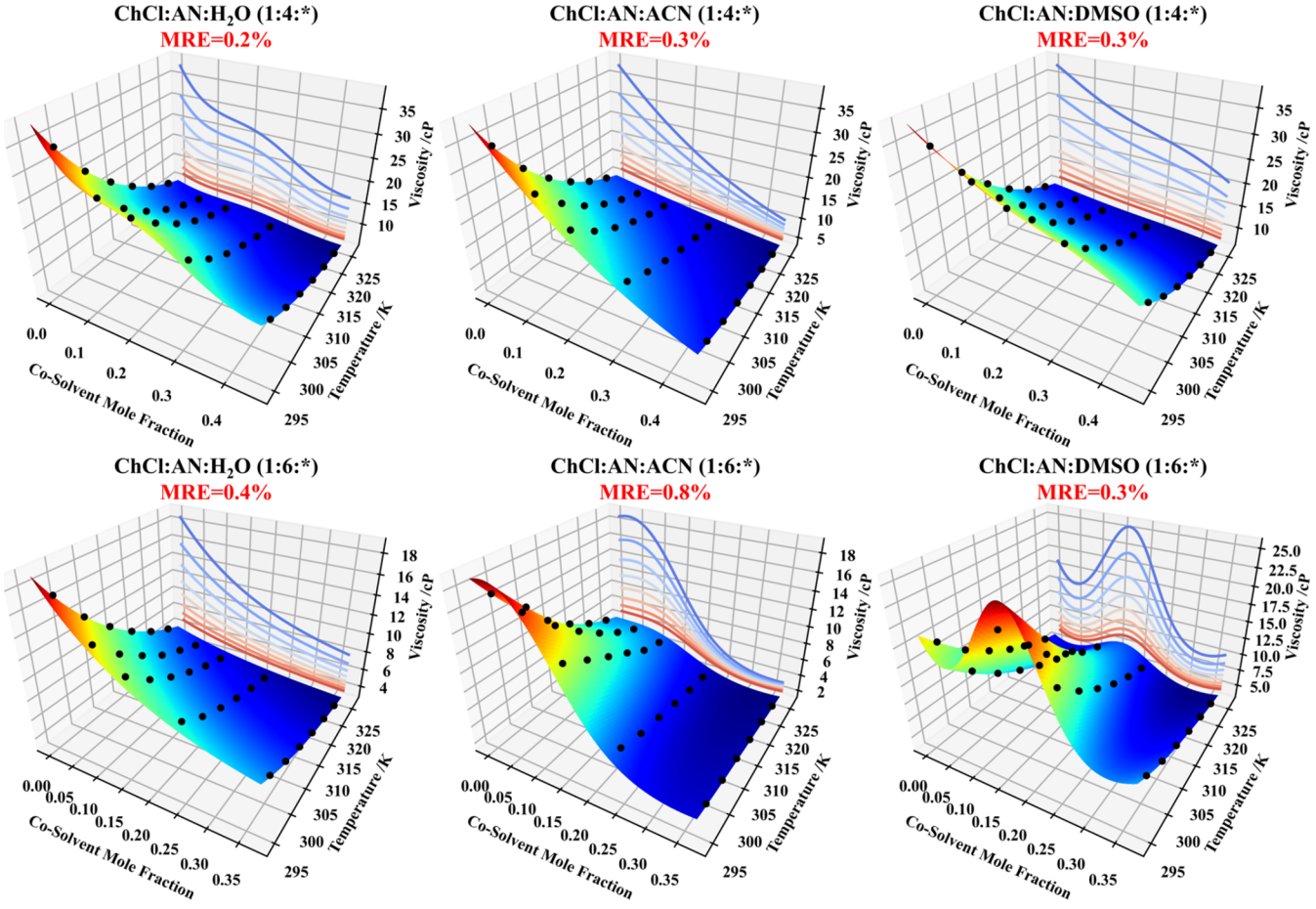


**Figure 3.** Three-dimensional surface plots of the GP-predicted viscosity of ChCl:AN:$H_2O$ (left column), ChCl:AN:ACN (middle column), and ChCl:AN:DMSO (right column), with a ChCl:AN molar ratio of 1:4 (top row) or 1:6 (bottom row), as a function of cosolvent composition and temperature. Color warmth in the surface corresponds to increasing viscosity. Projections of the surface on the composition/viscosity plane are also included, with color warmth corresponding to increasing temperature. GPs were trained using an RBF kernel (with a white noise kernel and a trainable Gaussian likelihood) against min−max-scaled features and log-standardized labels, with MREs being provided for each case. Black circles indicate experimental GP training data.

(3.21%). Finally, both standardization (2.06%) and log-standardization (2.25%) perform well and are superior to no label normalization (3.88%), although log-standardization better captures the natural distribution of viscosity values



https://doi.org/10.1021/acssuschemeng.4c04507
ACS Sustainable Chem. Eng. 2024, 12, 14218−14229

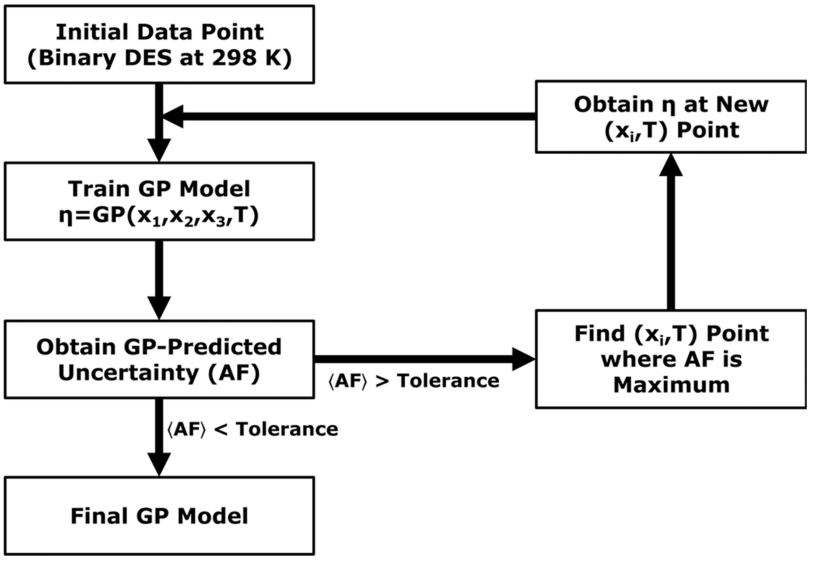


**Figure 4.** Schematic illustration of the active learning workflow employed in this work to iteratively construct GP models for the description of DES viscosities. Note how each new data point is selected based on the estimate of the model regarding its own uncertainty (acquisition function).

with respect to temperature while preventing unphysical viscosity predictions (e.g., negative values).

Given the results discussed above, features and labels were normalized with min−max scaling eq 10 and log-standardization eq 12, respectively. GPs were employed with an RBF kernel (in addition to a white noise kernel and a trainable Gaussian likelihood, yielding a total of four model hyperparameters). The results of fitting a GP to each ChCl:EG-based DES reported in the previous section are depicted in Figure 2 as three-dimensional plots and in Figure S1 as composition slices. GP hyperparameters are listed in Table S6.

Figure 2 reveals that GPs can accurately interpolate the viscosity of ternary DESs as a function of composition and temperature, with MREs comparable to those reported in Figure 1 for VFT fits. Note, however, that GPs here are being trained against all data points, yielding one model per system, while a new VFT fit is necessary for each composition slice. Thus, GPs retain model generality (by simultaneously interpolating across compositions and temperature) without any significant loss of accuracy when compared against the state-of-the-art viscosity correlative model.

The capability of GPs to describe viscosity data, as illustrated in Figure 2, allows for an extensive analysis of the impact of cosolvent composition on DES viscosities. ACN was the most effective cosolvent in lowering the viscosities of the studied EG-based DESs, with their values following an exponential decrease with respect to cosolvent composition. This trend is not readily seen for $H_2O$ or DMSO, where viscosities appear to decay linearly with the added cosolvent. This is consistent with the viscosities of the pure cosolvents, with ACN displaying a much lower viscosity (0.34 cP at 298 K)[47] than water (0.89 cP at 298 K)[43] or DMSO (1.99 cP at 298 K).[48]

While ACN is clearly the most efficient cosolvent to reduce the viscosity of ChCl:EG-based solvents, the trend for water and DMSO is not as clear. For example, at 298 K, the viscosity of neat ChCl:EG decreased from 20.9 to 10.8 cP in ChCl:EG:ACN 1:4:1 to 15.6 cP in ChCl:EG:DMSO 1:4:1 and to 17.0 cP in ChCl:EG:$H_2O$ 1:4:1 (Tables S1 and S2). Despite possessing a pure-component viscosity that is more than twice that of water, DMSO appears to rival the capacity for DES viscosity reduction of water. This is most likely connected to the ability of water to establish and participate in the hydrogen-bonding network of the neat ChCl:EG DES, whereas DMSO (much like ACN) possesses no hydrogen-bond-donating capability and is thus not expected to have relevant interactions with ChCl.

Having studied the impact of cosolvent addition on the viscosity of neat ChCl:EG, aniline-based DESs are now examined as three-dimensional plots in Figure 3 and as composition slices in Figure S2. Starting with the 1:4 mol ratio of ChCl/AN, ACN again provides the largest viscosity decrease with an exponential decay trend much like that seen in the ChCl:EG:ACN system (Figure 2). However, water now has a more pronounced effect on viscosity than DMSO, despite a faint inflection in its dependence on the cosolvent composition. For the smallest cosolvent mole fraction studied (0.5), water provides a viscosity decrease that is more pronounced than that provided by ACN (Table S3).

Contrary to ChCl:EG and 1:4 ChCl:AN, the addition of ACN or DMSO to 1:6 ChCl:AN leads to viscosity trends that are not monotonous, displaying relative extrema. In the case of ChCl:AN:ACN, this leads to an initial region where viscosity decreases slowly or stays approximately constant, followed by a sharp decrease with an increased ACN composition, a phenomenon that can be attributed to a disruption of the hydrogen-bonding network and subsequently the eutectic behavior of the solvents.[30] As previously discussed, this phenomenon arises from specific changes in the intermolecular interactions of DESs in the presence of cosolvents at particular mole fractions. These modifications entail alterations in the strength and number of hydrogen bonds between the HBD and HBA, which are attributed to the preference of either the HBD or HBA to interact and form hydrogen bonds with the cosolvent. Consequently, with high polarity cosolvents,[43] the cosolvent accumulates around the polar groups in the DES, significantly altering the solvation environment and weakening the HBD−HBA interactions, as described in analogous studies.[50,51]

As for ChCl:AN:DMSO, there is one clear viscosity maximum and two minima. Despite the complex behavior of


https://doi.org/10.1021/acssuschemeng.4c04507
ACS Sustainable Chem. Eng. 2024, 12, 14218−14229

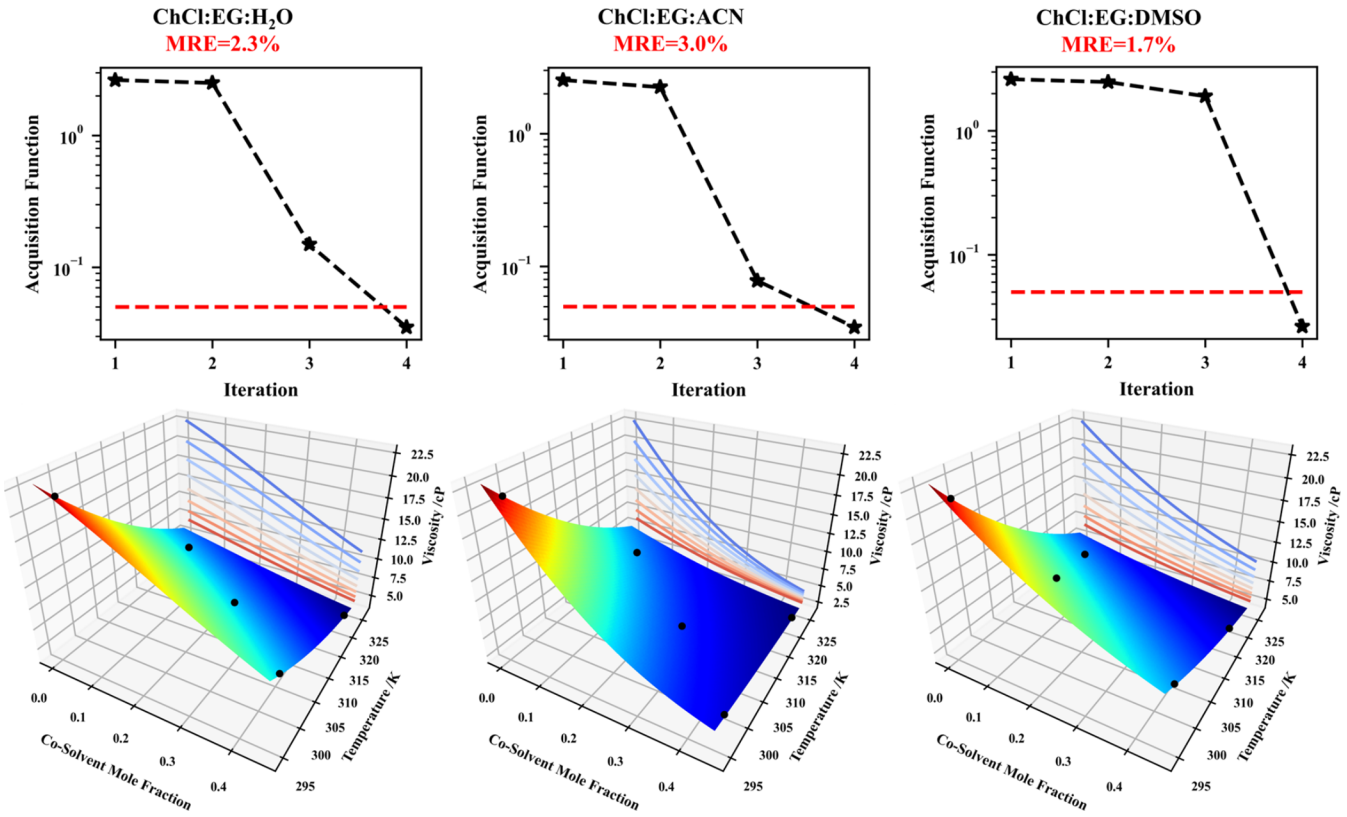


**Figure 5.** Active learning acquisition function with respect to AL iteration (top row), as well as three-dimensional surface plots of the GP-predicted viscosity (bottom row) for ChCl:EG:$H_2O$ (left column), ChCl:EG:ACN (middle column), and ChCl:EG:DMSO (right column) as a function of cosolvent composition and temperature. Color warmth in the surface corresponds to increasing viscosity. Projections of the surface on the composition/viscosity plane are also included, with color warmth corresponding to increasing temperature. GPs were trained on the active-learning-acquired data points highlighted (black circles), using an RBF kernel (with a white noise kernel and a trainable Gaussian likelihood) against min−max-scaled features and log-standardized labels, with MREs being provided for each case.

these three-dimensional viscosity surfaces, GPs can accurately describe them, with MREs on par or even superior to those reported in Figure 1 for VFT fits.

While understanding and interpreting the nonmonotonic behavior of viscosity for ChCl:AN:ACN and ChCl:AN:DMSO from a molecular perspective is beyond the scope of this work, it is worth noting that such behavior has been previously observed in the literature for other DES properties. Examples include activity coefficient[52] and hydrogen-bonding number[53] extrema for ChCl:urea and ChCl:betaine with the addition of small quantities of water. There is also limited evidence of a small inflection in the behavior of the viscosity for the same system with the addition of water.[54] This type of unusual viscosity behavior is often overlooked and seldom reported in the DES literature, most likely due to a lack of composition-dependent viscosity models. This hinders a comprehensive analysis, which the usage of GPs fully resolves.

**Active Learning.** The results reported in the previous section establish GPs as accurate and useful models to correlate and interpolate DES viscosity data as a function of all operational conditions of interest, particularly cosolvent composition and temperature. However, the applicability of GPs does not lie solely in data regression. As explained earlier, GPs provide uncertainty estimates for their own label predictions eq 9. This can be leveraged to develop AL algorithms that build GP models in an iterative fashion, a technique already tested on highly data-efficient phase diagram construction for DESs.[28] That is, rather than performing high-throughput experimental screenings on predefined, fine composition/temperature data meshes, viscosity data sets can be built sequentially. An initial viscosity data point is measured (that of the neat DES at room temperature), and a GP model is trained on that single data point. Then, eq 9 is used to compute uncertainty estimates across the composition and temperature ranges of interest, and the composition/temperature testing point with maximal uncertainty (or another variance-derived metric of interest) is probed experimentally. This new experimental viscosity data point is then added to the available data set, the GP model is retrained, and new uncertainty estimates are computed, yielding the next experimental viscosity point to measure. The active learning algorithm continues until the metric of interest is below a given threshold, as schematized in Figure 4.

The acquisition function (AF) chosen in this work is the GP-predicted relative error, defined as

$$\mathrm{AF} = \frac{\sqrt{\Sigma'}}{\mu'} \tag{14}$$

where $\sum'$ and $\mu'$ follow from the definitions of eqs 8 and 9 and represent the GP-predicted variance and mean, respectively. The stopping criterion chosen was an average AF value of 5%. Thus, the active learning algorithm halts when the GP-predicted mean relative error is below 5% rather than stopping when a prearranged number of experimental data points has been collected. The results for the EG-based DESs studied thus far are reported in Figure 5, including the convergence of


https://doi.org/10.1021/acssuschemeng.4c04507
ACS Sustainable Chem. Eng. 2024, 12, 14218−14229

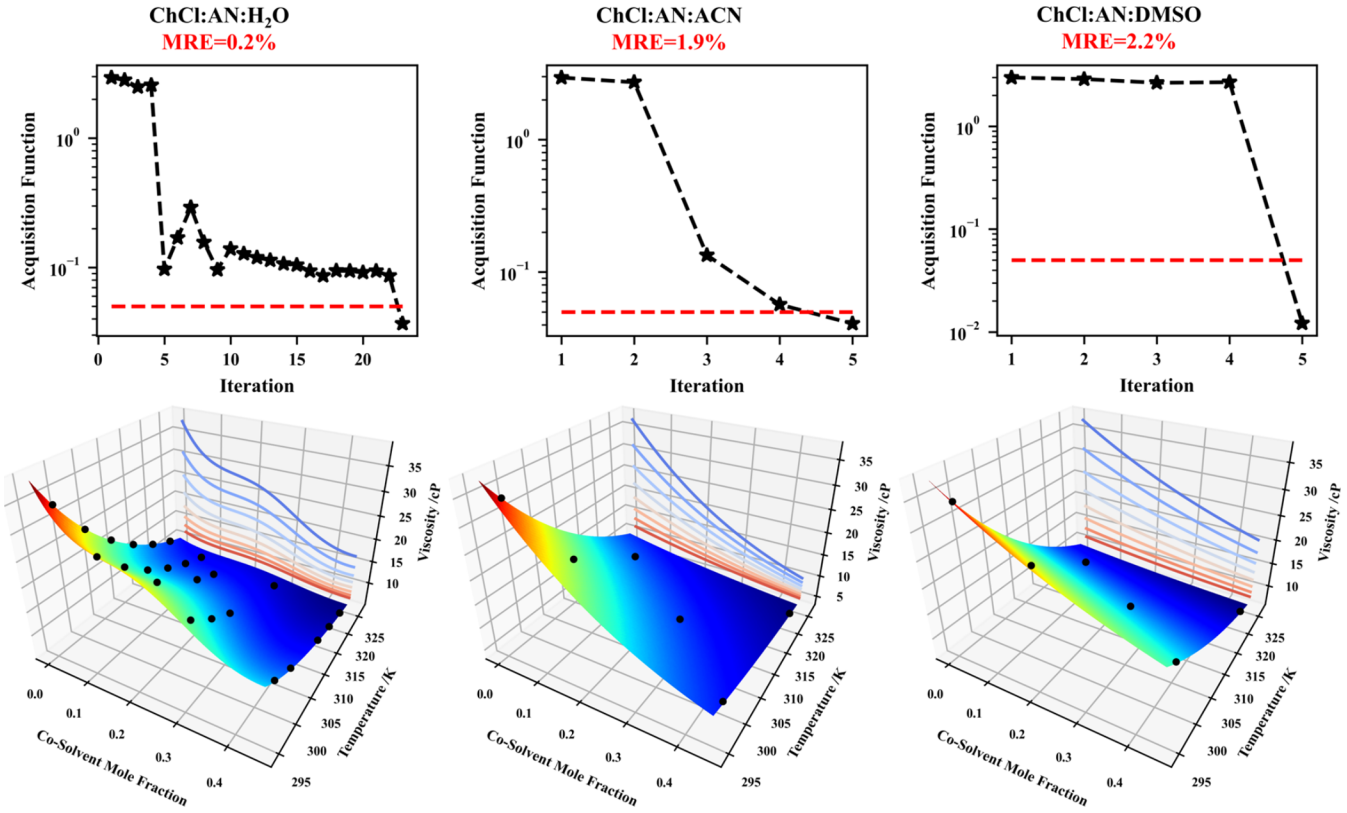


**Figure 6.** Active learning acquisition function with respect to AL iteration (top row), as well as three-dimensional surface plots of the GP-predicted viscosity (bottom row) for ChCl:AN:$H_2O$ (1:4:*) (left column), ChCl:AN:ACN (1:4:*) (middle column), and ChCl:AN:DMSO (1:4:*) (right column) as a function of cosolvent composition and temperature. Color warmth in the surface corresponds to increasing viscosity. Projections of the surface on the composition/viscosity plane are also included, with color warmth corresponding to increasing temperature. GPs were trained on the active-learning-acquired data points highlighted (black circles), using an RBF kernel (with a white noise kernel and a trainable Gaussian likelihood) against min−max-scaled features and log-standardized labels, with MREs being provided for each case.

AF as a function of AL iteration. Composition slices, along with the progression of AL-acquired data points, are provided in Figure S3.

The performance of AL reported in Figure 5 is remarkable. With no experimental input beyond the viscosity of neat DES ChCl:EG at room temperature, AL acquires four additional experimental viscosity data points and halts, attaining an average acquisition function below the requested 5%. In turn, this leads to GP models that although are only trained on five experimental data points, they accurately describe the three-dimensional viscosity−temperature−composition surface of each system, with MREs (computed based on all available data, not just the active-learning-acquired training data fed to the GPs) between 1.7% for ChCl:EG:DMSO and 3.0% for ChCl:EG:ACN. This represents a 6-fold reduction in the amount of data initially measured without AL to describe the viscosity of these systems and establishes AL as a powerful and useful tool for data reduction.

Having examined the results for EG-based DESs, we now discuss their aniline counterparts. It is worth noting that ChCl/AN (both in the 1:4 and 1:6 molar ratios) presented complex behavior, with nonmonotonic composition dependencies of viscosity in some cases, as discussed in the previous section. Thus, both molar ratios are analyzed separately, starting with the 1:4 molar ratio in Figure 6 and the 1:6 molar ratio in Figure 7. Similar to ChCl:EG, Figures S4 and S5 depict composition slices and AL data progression for each case, respectively.

The performance of AL for ChCl:AN:ACN (1:4:*) and ChCl:AN:DMSO (1:4:*) reported in Figure 6 is similar to that seen for ChCl:EG in Figure 5, with only 6 experimental viscosity data points being necessary to fully describe the viscosity surfaces of interest, attaining MREs of 1.9 and 2.2%, respectively. In stark contrast, AL takes 23 iterations to converge to a mean acquisition function of 5% for ChCl:AN:$H_2O$ (1:4:*). This lower performance is most likely connected to the unusual inflection points seen in the temperature slices of this system (Figure 3), leading to a viscosity surface that possesses a saddle point and, thus, is more difficult to capture. Nevertheless, the GPs trained throughout the AL workflow for this system capture that unusual behavior by providing larger uncertainty estimates to AL, which in turn requests more experimental data. Of course, the data requirements for this system can be significantly decreased by simply increasing the requested stopping criterion leading, naturally, to a larger MRE.

The final AL case study analyzed in this work is that of the systems based on neat ChCl/AN (1:6), as reported in Figure 7. Unlike ChCl:AN:$H_2O$ (1:4:*), AL converges to an accurate representation of viscosity (MRE of 1.4%) for ChCl:AN:$H_2O$ (1:6:*) in just 5 iterations, much like the results seen for the remaining ternary systems based on ChCl/AN (1:4) and ChCl:EG. This supports the notion that the poor performance of AL seen for ChCl:AN:$H_2O$ (1:4:*) in Figure 6 is unrelated to the cosolvent used, instead being connected with the saddle point of the overall viscosity surface.



https://doi.org/10.1021/acssuschemeng.4c04507
ACS Sustainable Chem. Eng. 2024, 12, 14218−14229

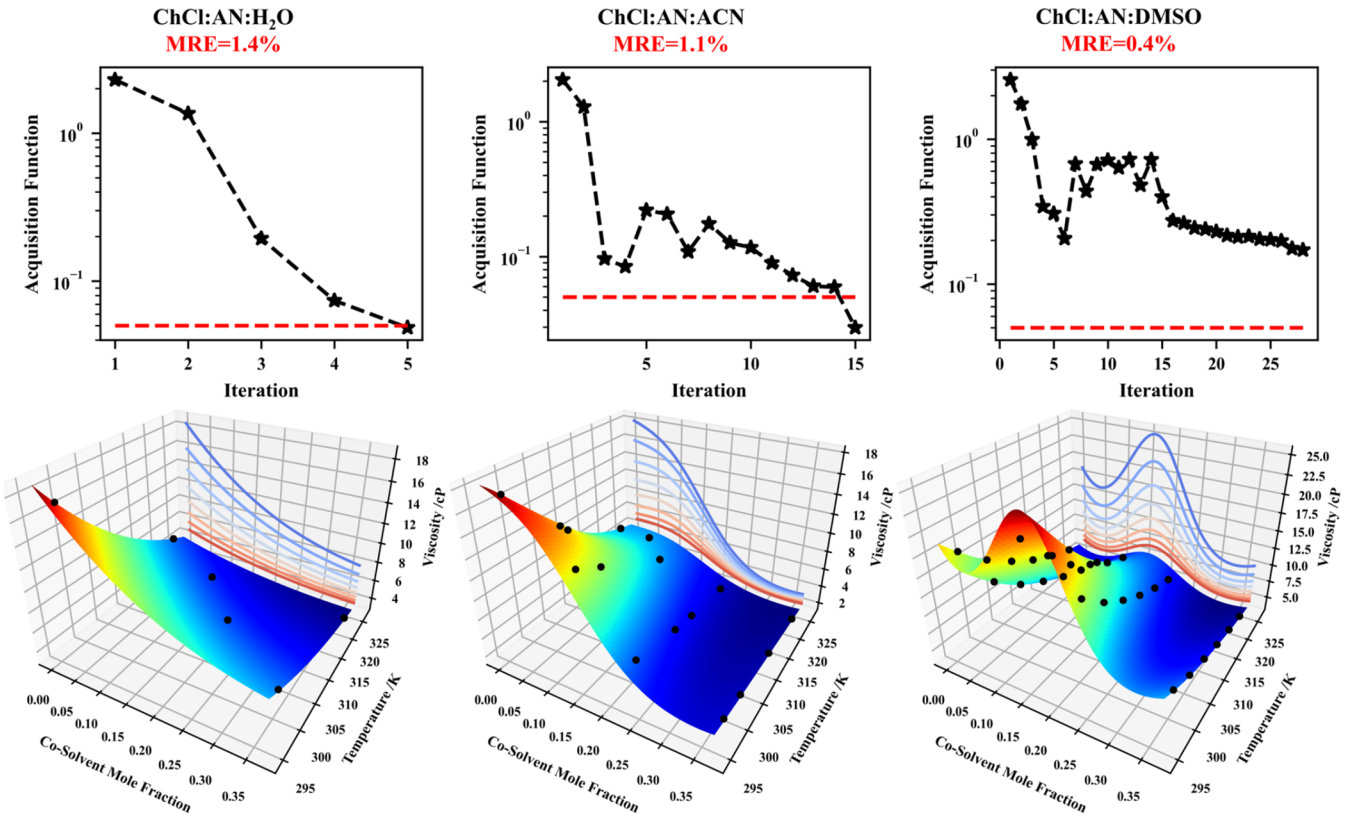


**Figure 7.** Active learning acquisition function with respect to AL iteration (top row), as well as three-dimensional surface plots of the GP-predicted viscosity (bottom row) for ChCl:AN:$H_2O$ (1:6:*) (left column), ChCl:AN:ACN (1:6:*) (middle column), and ChCl:AN:DMSO (1:6:*) (right column) as a function of cosolvent composition and temperature. Color warmth in the surface corresponds to increasing viscosity. Projections of the surface on the composition/viscosity plane are also included, with color warmth corresponding to increasing temperature. GPs were trained on the active-learning-acquired data points highlighted (black circles), using an RBF kernel (with a white noise kernel and a trainable Gaussian likelihood) against min−max-scaled features and log-standardized labels, with MREs being provided for each case.

The AL behavior for ChCl:AN:ACN (1:6:*) and ChCl:AN:DMSO (1:6:*) is particularly interesting and similar to that observed for ChCl:AN:$H_2O$ (1:4:*). In the first case, the GP-derived acquisition function quickly reaches 10% and then oscillates between 10 and 20% until iteration 14, where the algorithm is finally satisfied with its understanding of the viscosity surface of the system and its nonmonotonic behavior. Similarly, the acquisition function for ChCl:AN:DMSO (1:6:*) fluctuates between roughly 20 and 70%, eventually reaching roughly 10% when there are no more experimental data points to acquire. Thus, ChCl:AN:DMSO (1:6:*) is the only system where AL fails to outperform the data requirements of the high-throughput experimental screening reported earlier. However, there is merit in the ability of the underlying GP to understand that the viscosity surface is complex and nonmonotonic and the translation of this into an acquisition function that is considerably larger than those seen for the remaining systems. This is an important advantage of AL that, despite not necessarily leading to greater experimental acquisition efficiency, allows for the quick identification of problematic systems with outlying behavior that, depending on the application, warrants closer examination.

The AL results reported in this section demonstrate the major advantages of using GP-based tools to correlate viscosity data for DESs and guide the acquisition of experimental data. This leads to an experimentally inexpensive exploration of the DES design space, requiring the measurement of only those viscosity data points that are strictly necessary to obtain an accurate GP model and eliminating redundancies. This, combined with our previous results that demonstrated the feasibility of applying AL to describe activity coefficients and phase equilibria for DESs,[28] shows that AL is a valuable and general tool for data reduction targeting DES development and design.

## CONCLUSIONS

In this work, a high-throughput experimental screening was performed to measure the viscosity of three neat DESs—ChCl:EG, ChCl:AN (1:4), and ChCl:AN (1:6)—and their mixtures therein with three low-molecular-weight cosolvents, water, acetonitrile, and DMSO, aiming at developing semi-empirical tools to accelerate the design and development of DESs. The high-throughput experimental data obtained were also validated using the VFT equation, and temperature trends were discussed.

GPs were able to fully interpolate and describe the viscosity data measured for the nine ternary DES systems studied. Owing to their ability of capturing both composition and temperature dependencies, the usage of GPs allowed the identification of the best cosolvents to decrease the viscosity of a particular neat DES, as well as unexpected nonmonotonic trends between the amount of added cosolvent and DES viscosities.

The ability of GPs to estimate the uncertainty of their predictions was leveraged in an AL workflow, aiming at minimizing the amount of experimental data necessary to


https://doi.org/10.1021/acssuschemeng.4c04507
ACS Sustainable Chem. Eng. 2024, 12, 14218−14229

describe the relationship between DES viscosity and cosolvent composition/temperature. A substantial efficiency increase was attained for several systems, particularly those based on ethylene glycol where only five experimental data points, acquired through AL, were necessary to fully describe the overall viscosity data set in each case. This represented a 6-fold increase in efficiency when compared with the high-throughput experimental screening based on a predetermined temperature/composition grid.

All in all, we demonstrated that leveraging the combined approach of AL and high-throughput screenings greatly enhances the efficiency of experimentally characterizing the physicochemical properties of DESs. Owing to their stochastic nature and the GP inputs chosen (composition and temperature), the performance of the AL methodology presented in this work is mostly affected by the shape of the viscosity surface (as demonstrated in Figures 5−7) rather than the chemical nature of the mixture components. Thus, the results and conclusions obtained are expected to be general and valid across other ternary DESs and HBD/HBA/cosolvent combinations.

## ■ ASSOCIATED CONTENT

### Supporting Information

The Supporting Information is available free of charge at https://pubs.acs.org/doi/10.1021/acssuschemeng.4c04507.

Different ways of visualizing the GP and active learning results reported in the main text (Figures S1−S5); experimental data measured in this work (Tables S1−S4); and additional GP results (Tables S5 and S6) (PDF)

## ■ AUTHOR INFORMATION


### Corresponding Author

**Yamil J. Colón** − *Department of Chemical and Biomolecular Engineering, University of Notre Dame, Notre Dame, Indiana 46556, United States;* orcid.org/0000-0001-5316-9692; Email: ycolon@nd.edu

### Authors

**Dinis O. Abranches** − *Department of Chemical and Biomolecular Engineering, University of Notre Dame, Notre Dame, Indiana 46556, United States;* orcid.org/0000-0003-0097-2072

**William Dean** − *Chemical and Biomolecular Engineering Department, Case Western Reserve University, Cleveland, Ohio 44106, United States*

**Miguel Muñoz** − *Chemical and Biomolecular Engineering Department, Case Western Reserve University, Cleveland, Ohio 44106, United States*

**Wei Wang** − *Pacific Northwest National Laboratory, Richland, Washington 99354, United States;* orcid.org/0000-0002-5453-4695

**Yangang Liang** − *Pacific Northwest National Laboratory, Richland, Washington 99354, United States;* orcid.org/0000-0001-6712-3695

**Burcu Gurkan** − *Chemical and Biomolecular Engineering Department, Case Western Reserve University, Cleveland, Ohio 44106, United States;* orcid.org/0000-0003-4886-3350

**Edward J. Maginn** − *Department of Chemical and Biomolecular Engineering, University of Notre Dame, Notre Dame, Indiana 46556, United States;* orcid.org/0000-0002-6309-1347

Complete contact information is available at: https://pubs.acs.org/10.1021/acssuschemeng.4c04507


### Notes

The authors declare no competing financial interest.

## ■ ACKNOWLEDGMENTS

This work was supported by the Breakthrough Electrolytes for Energy Storage Systems (BEES2), an Energy Frontier Research Center funded by the U.S. Department of Energy, Office of Science, Basic Energy Sciences (BES), under award DE-SC0019409. The authors acknowledge the Center for Research Computing (CRC) at the University of Notre Dame for providing computational resources. D.O.A. also thanks the support of the Patrick and Jana Eilers Graduate Student Fellowship for Energy Related Research. The authors also acknowledge the support from the Automated Robotics for Energy Storage Laboratory (ARES Lab) funded by the Energy Storage Materials Initiative (ESMI), which is a Laboratory Directed Research and Development Project at Pacific Northwest National Laboratory (PNNL).

## ■ REFERENCES


(1) Abranches, D. O.; Coutinho, J. A. P. Everything You Wanted to Know about Deep Eutectic Solvents but Were Afraid to Be Told. *Annu. Rev. Chem. Biomol. Eng.* **2023**, *14* (1), 141−163.

(2) Hansen, B. B.; Spittle, S.; Chen, B.; Poe, D.; Zhang, Y.; Klein, J. M.; Horton, A.; Adhikari, L.; Zelovich, T.; Doherty, B. W.; Gurkan, B.; Maginn, E. J.; Ragauskas, A.; Dadmun, M.; Zawodzinski, T. A.; Baker, G. A.; Tuckerman, M. E.; Savinell, R. F.; Sangoro, J. R. Deep Eutectic Solvents: A Review of Fundamentals and Applications. *Chem. Rev.* **2021**, *121* (3), 1232−1285.

(3) Prabhune, A.; Dey, R. Green and Sustainable Solvents of the Future: Deep Eutectic Solvents. *J. Mol. Liq.* **2023**, *379*, No. 121676.

(4) García, G.; Aparicio, S.; Ullah, R.; Atilhan, M. Deep Eutectic Solvents: Physicochemical Properties and Gas Separation Applications. *Energy Fuels* **2015**, *29* (4), 2616−2644.

(5) Trivedi, T. J.; Lee, J. H.; Lee, H. J.; Jeong, Y. K.; Choi, J. W. Deep Eutectic Solvents as Attractive Media for $CO_2$ Capture. *Green Chem.* **2016**, *18* (9), 2834−2842.

(6) Zainal-Abidin, M. H.; Hayyan, M.; Hayyan, A.; Jayakumar, N. S. New Horizons in the Extraction of Bioactive Compounds Using Deep Eutectic Solvents: A Review. *Anal. Chim. Acta* **2017**, *979*, 1−23.

(7) Bubalo, M. C.; Ćurko, N.; Tomašević, M.; Ganić, K. K.; Redovniković, I. R. Green Extraction of Grape Skin Phenolics by Using Deep Eutectic Solvents. *Food Chem.* **2016**, *200*, 159−166.

(8) Ruesgas-Ramón, M.; Figueroa-Espinoza, M. C.; Durand, E. Application of Deep Eutectic Solvents (DES) for Phenolic Compounds Extraction: Overview, Challenges, and Opportunities. *J. Agric. Food Chem.* **2017**, *65* (18), 3591−3601.

(9) Cunha, S. C.; Fernandes, J. O. Extraction Techniques with Deep Eutectic Solvents. *TrAC, Trends Anal. Chem.* **2018**, *105*, 225−239.

(10) Abbott, A. P.; Capper, G.; Davies, D. L.; McKenzie, K. J.; Obi, S. U. Solubility of Metal Oxides in Deep Eutectic Solvents Based on Choline Chloride. *J. Chem. Eng. Data* **2006**, *51* (4), 1280−1282.

(11) Richter, J.; Ruck, M. Synthesis and Dissolution of Metal Oxides in Ionic Liquids and Deep Eutectic Solvents. *Molecules* **2020**, *25* (1), No. 78.

(12) Pedro, S. N.; Freire, M. G.; Freire, C. S. R.; Silvestre, A. J. D. Deep Eutectic Solvents Comprising Active Pharmaceutical Ingredients in the Development of Drug Delivery Systems. *Expert Opin. Drug Delivery* **2019**, *16* (5), 497−506.

(13) Emami, S.; Shayanfar, A. Deep Eutectic Solvents for Pharmaceutical Formulation and Drug Delivery Applications. *Pharm. Dev. Technol.* **2020**, *25* (7), 779−796.
(14) Abbott, A. P. Deep Eutectic Solvents and Their Application in Electrochemistry. *Curr. Opin. Green Sustainable Chem.* **2022**, *36*, No. 100649.
(15) Wu, J.; Liang, Q.; Yu, X.; Lü, Q.; Ma, L.; Qin, X.; Chen, G.; Li, B. Deep Eutectic Solvents for Boosting Electrochemical Energy Storage and Conversion: A Review and Perspective. *Adv. Funct. Mater.* **2021**, *31* (22), No. 2011102, DOI: 10.1002/adfm.202011102.
(16) Ghahremani, R.; Savinell, R. F.; Gurkan, B. Perspective—Hydrogen Bonded Concentrated Electrolytes for Redox Flow Batteries: Limitations and Prospects. *J. Electrochem. Soc.* **2022**, *169* (3), No. 030520.
(17) Chakrabarti, M. H.; Mjalli, F. S.; AlNashef, I. M.; Hashim, M. A.; Hussain, M. A.; Bahadori, L.; Low, C. T. J. Prospects of Applying Ionic Liquids and Deep Eutectic Solvents for Renewable Energy Storage by Means of Redox Flow Batteries. *Renewable Sustainable Energy Rev.* **2014**, *30*, 254−270.
(18) Gygli, G.; Xu, X.; Pleiss, J. Meta-Analysis of Viscosity of Aqueous Deep Eutectic Solvents and Their Components. *Sci. Rep.* **2020**, *10* (1), No. 21395.
(19) Gajardo-Parra, N. F.; Cotroneo-Figueroa, V. P.; Aravena, P.; Vesovic, V.; Canales, R. I. Viscosity of Choline Chloride-Based Deep Eutectic Solvents: Experiments and Modeling. *J. Chem. Eng. Data* **2020**, *65* (11), 5581−5592.
(20) Zhang, Y.; Poe, D.; Heroux, L.; Squire, H.; Doherty, B. W.; Long, Z.; Dadmun, M.; Gurkan, B.; Tuckerman, M. E.; Maginn, E. J. Liquid Structure and Transport Properties of the Deep Eutectic Solvent Ethaline. *J. Phys. Chem. B* **2020**, *124* (25), 5251−5264.
(21) Yadav, A.; Pandey, S. Densities and Viscosities of (Choline Chloride + Urea) Deep Eutectic Solvent and Its Aqueous Mixtures in the Temperature Range 293.15 to 363.15 K. *J. Chem. Eng. Data* **2014**, *59* (7), 2221−2229.
(22) Sarmad, S.; Xie, Y.; Mikkola, J.-P.; Ji, X. Screening of Deep Eutectic Solvents (DESs) as Green $CO_2$ Sorbents: From Solubility to Viscosity. *New J. Chem.* **2017**, *41* (1), 290−301.
(23) Ma, C.; Laaksonen, A.; Liu, C.; Lu, X.; Ji, X. The Peculiar Effect of Water on Ionic Liquids and Deep Eutectic Solvents. *Chem. Soc. Rev.* **2018**, *47* (23), 8685−8720.
(24) Al-Dawsari, J. N.; Bessadok-Jemai, A.; Wazeer, I.; Mokraoui, S.; AlMansour, M. A.; Hadj-Kali, M. K. Fitting of Experimental Viscosity to Temperature Data for Deep Eutectic Solvents. *J. Mol. Liq.* **2020**, *310*, No. 113127.
(25) Bakhtyari, A.; Haghbakhsh, R.; Duarte, A. R. C.; Raeissi, S. A Simple Model for the Viscosities of Deep Eutectic Solvents. *Fluid Phase Equilib.* **2020**, *521*, No. 112662.
(26) Rasmussen, C. E.; Williams, C. K. I. *Gaussian Processes for Machine Learning*, 2nd ed.; The MIT Press, 2006.
(27) Deringer, V. L.; Bartók, A. P.; Bernstein, N.; Wilkins, D. M.; Ceriotti, M.; Csányi, G. Gaussian Process Regression for Materials and Molecules. *Chem. Rev.* **2021**, *121* (16), 10073−10141.
(28) Abranches, D. O.; Maginn, E. J.; Colón, Y. J. Activity Coefficient Acquisition with Thermodynamics-informed Active Learning for Phase Diagram Construction. *AIChE J.* **2023**, *69* (8), No. e18141, DOI: 10.1002/aic.18141.
(29) Mukherjee, K.; Osaro, E.; Colón, Y. J. Active Learning for Efficient Navigation of Multi-Component Gas Adsorption Landscapes in a MOF. *Digital Discovery* **2023**, *2* (5), 1506−1521.
(30) Dean, W.; Muñoz, M.; Noh, J.; Liang, Y.; Wang, W.; Gurkan, B. Tuning and High Throughput Experimental Screening of Eutectic Electrolytes with Co-Solvents for Redox Flow Batteries. *Electrochim. Acta* **2024**, *474*, No. 143517.
(31) Liang, Y.; Job, H.; Feng, R.; Parks, F.; Hollas, A.; Zhang, X.; Bowden, M.; Noh, J.; Murugesan, V.; Wang, W. High-Throughput Solubility Determination for Data-Driven Materials Design and Discovery in Redox Flow Battery Research. *Cell Rep. Phys. Sci.* **2023**, *4* (10), No. 101633.
(32) Noh, J.; Doan, H. A.; Job, H.; Robertson, L. A.; Zhang, L.; Assary, R. S.; Mueller, K.; Murugesan, V.; Liang, Y. An Integrated High-Throughput Robotic Platform and Active Learning Approach for Accelerated Discovery of Optimal Electrolyte Formulations. *Nat. Commun.* **2024**, *15* (1), No. 2757.
(33) Garca-Coln, L. S.; del Castillo, L. F.; Goldstein, P. Theoretical Basis for the Vogel-Fulcher-Tammann Equation. *Phys. Rev. B* **1989**, *40* (10), No. 7040.
(34) Rasmussen, C. E.Gaussian Processes in Machine Learning. In *Lecture Notes in Computer Science*; Springer, 2004; Vol. *3176*, pp 63−71.
(35) Duvenaud, D. Automatic Model Construction with Gaussian Processes, Ph.D. Thesis; University of Cambridge, 2014.
(36) de G Matthews, A. G.; van der Wilk, M.; Nickson, T.; Fujii, K.; Boukouvalas, A.; León-Villagrá, P.; Ghahramani, Z.; Hensman, J. GPflow: A Gaussian Process Library Using TensorFlow. *J. Mach. Learn. Res.* **2017**, *18* (40), 1−6.
(37) Developers, T. *TensorFlow*; Zenodo, 2023.
(38) Abadi, M.; Agarwal, A.; Barham, P.; Brevdo, E.; Chen, Z.; Citro, C.; Corrado, G. S.; Davis, A.; Dean, J.; Devin, M.; Ghemawat, S.; Goodfellow, I.; Harp, A.; Irving, G.; Isard, M.; Jia, Y.; Jozefowicz, R.; Kaiser, L.; Kudlur, M.; Levenberg, J.; Mane, D.; Monga, R.; Moore, S.; Murray, D.; Olah, C.; Schuster, M.; Shlens, J.; Steiner, B.; Sutskever, I.; Talwar, K.; Tucker, P.; Vanhoucke, V.; Vasudevan, V.; Viegas, F.; Vinyals, O.; Warden, P.; Wattenberg, M.; Wicke, M.; Yu, Y.; Zheng, X. TensorFlow: Large-Scale Machine Learning on Heterogeneous Distributed Systems, arXiv:1603.04467. arXiv.org e-Print archive, 2016. https://arxiv.org/abs/1603.04467.
(39) Byrd, R. H.; Lu, P.; Nocedal, J.; Zhu, C. A Limited Memory Algorithm for Bound Constrained Optimization. *SIAM J. Sci. Comput.* **1995**, *16* (5), 1190−1208.
(40) Shastan, F. Z.; Nowroozi, A. Thermophysical and Transport Properties of Deep Eutectic Solvent Mixtures Containing Pure Choline Chloride/Ethylene Glycol with a Mole Ratio of 1:4 and Mixed with LiPF6 for Application in Redox-flow Batteries. *Preprints* **2023**, No. 2023111148.
(41) Mjalli, F. S.; Naser, J. Viscosity Model for Choline Chloride-based Deep Eutectic Solvents. *Asia-Pac. J. Chem. Eng.* **2015**, *10* (2), 273−281.
(42) Alfurayj, I.; Fraenza, C. C.; Zhang, Y.; Pandian, R.; Spittle, S.; Hansen, B.; Dean, W.; Gurkan, B.; Savinell, R.; Greenbaum, S.; Maginn, E.; Sangoro, J.; Burda, C. Solvation Dynamics of Wet Ethaline: Water Is the Magic Component. *J. Phys. Chem. B* **2021**, *125* (31), 8888−8901.
(43) Wang, Y.; Ma, C.; Liu, C.; Lu, X.; Feng, X.; Ji, X. Thermodynamic Study of Choline Chloride-Based Deep Eutectic Solvents with Water and Methanol. *J. Chem. Eng. Data* **2020**, *65* (5), 2446−2457.
(44) Lapeña, D.; Lomba, L.; Artal, M.; Lafuente, C.; Giner, B. Thermophysical Characterization of the Deep Eutectic Solvent Choline Chloride:Ethylene Glycol and One of Its Mixtures with Water. *Fluid Phase Equilib.* **2019**, *492*, 1−9.
(45) Lien, C.-W.; Vedhanarayanan, B.; Chen, J.-H.; Lin, J.-Y.; Tsai, H.-H.; Shao, L.-D.; Lin, T.-W. Optimization of Acetonitrile/Water Content in Hybrid Deep Eutectic Solvent for Graphene/MoS2 Hydrogel-Based Supercapacitors. *Chem. Eng. J.* **2021**, *405*, No. 126706.
(46) Harifi-Mood, A. R.; Buchner, R. Density, Viscosity, and Conductivity of Choline Chloride + Ethylene Glycol as a Deep Eutectic Solvent and Its Binary Mixtures with Dimethyl Sulfoxide. *J. Mol. Liq.* **2017**, *225*, 689−695.
(47) Paez, S.; Contreras, M. Densities and Viscosities of Binary Mixtures of 1-Propanol and 2-Propanol with Acetonitrile. *J. Chem. Eng. Data* **1989**, *34* (4), 455−459.
(48) Govinda, V.; Attri, P.; Venkatesu, P.; Venkateswarlu, P. Temperature Effect on the Molecular Interactions between Two Ammonium Ionic Liquids and Dimethylsulfoxide. *J. Mol. Liq.* **2011**, *164* (3), 218−225.

(49) Zuo, Z.; Cao, B.; Wang, Y.; Ma, C.; Lu, X.; Ji, X. Thermodynamic Study of Choline Chloride-Based Deep Eutectic Solvents with Dimethyl Sulfoxide and Isopropanol. *J. Mol. Liq.* **2024**, *394*, No. 123731.
(50) Zhekenov, T.; Toksanbayev, N.; Kazakbayeva, Z.; Shah, D.; Mjalli, F. S. Formation of Type III Deep Eutectic Solvents and Effect of Water on Their Intermolecular Interactions. *Fluid Phase Equilib.* **2017**, *441*, 43−48.
(51) Shah, D.; Mansurov, U.; Mjalli, F. S. Intermolecular Interactions and Solvation Effects of Dimethylsulfoxide on Type III Deep Eutectic Solvents. *Phys. Chem. Chem. Phys.* **2019**, *21* (31), 17200−17208.
(52) Abranches, D. O.; Silva, L. P.; Martins, M. A. R.; Coutinho, J. A. P. Differences on the Impact of Water on the Deep Eutectic Solvents Betaine/Urea and Choline/Urea. *J. Chem. Phys.* **2021**, *155* (3), No. 034501, DOI: 10.1063/5.0052303.
(53) Shah, D.; Mjalli, F. S. Effect of Water on the Thermo-Physical Properties of Reline: An Experimental and Molecular Simulation Based Approach. *Phys. Chem. Chem. Phys.* **2014**, *16* (43), 23900−23907.
(54) Al-Murshedi, A. Y. M.; Alesary, H. F.; Al-Hadrawi, R. Thermophysical Properties in Deep Eutectic Solvents with/without Water. *J. Phys.: Conf. Ser.* **2019**, *1294* (5), No. 052041.



https://doi.org/10.1021/acssuschemeng.4c04507
*ACS Sustainable Chem. Eng.* 2024, 12, 14218−14229